Direct CO2 laser-based generation of holographic structures on the surface of glass

Direct CO_2 laser-based generation of holographic structures on the surface of glass

Krystian L. Wlodarczyk,[1,*] Nicholas J. Weston,[2] Marcus Ardron,[2] and Duncan P. Hand[1]

[1]*Institute of Photonics and Quantum Sciences, School of Engineering and Physical Sciences, Heriot-Watt University, Edinburgh, EH11 4AS, UK*

[2]*Renishaw plc, Research Park North, Riccarton, Edinburgh, EH14 4AP, UK*

[*]*K.L.Wlodarczyk@hw.ac.uk*

Abstract: A customized CO_2 laser micromachining system was used for the generation of phase holographic structures directly on the surface of fused silica (HPFS®7980 Corning) and Borofloat®33 (Schott AG) glass. This process used pulses of duration 10μs and nominal wavelength 10.59μm. The pulse energy delivered to the glass workpiece was controlled by an acousto-optic modulator. The laser-generated structures were optically smooth and crack free. We demonstrated their use as diffractive optical elements (DOEs), which could be exploited as anti-counterfeiting markings embedded into valuable glass-made components and products.

OCIS codes: (090.1970) Diffractive optics; (140.3070) Infrared and far-infrared lasers; (140.3390) Laser materials processing; (160.2750) Glass and other amorphous materials; (220.4000) Microstructure fabrication.

References and links

1. K. L. Wlodarczyk, M. Ardron, A. J. Waddie, A. Dunn, M. D. Kidd, N. J. Weston, and D. P. Hand, "Laser microsculpting for the generation of robust diffractive security markings on the surface of metals," J. Mater. Process. Technol. **222**, 206–218 (2015).
2. "Laser marking of glass," *http://www.rofin.com/en/markets/glass-industry/laser-marking/*.
3. "Glass marking techniques using CO_2 lasers," *http://www.synrad.com/synradinside/pdfs/Glassmarkingmethods.pdf*.
4. F. Laguarta, N. Lupon, and J. Armengol, "Optical glass polishing by controlled laser surface-heat treatment," Appl. Opt. **33**(27), 6508–6513 (1994).
5. S. Heidrich, E. Willenborg, and A. Richmann, "Development of a laser based process chain for manufacturing freeform optics," Phys. Proc. **12**, 519–528 (2011).
6. K. M. Nowak, H. J. Baker, and D. R. Hall, "Efficient laser polishing of silica micro-optic components," Appl. Opt. **45**(1), 162–171 (2006).
7. J. F. Monjardin, K. M. Nowak, H. J. Baker, and D. R. Hall, "Correction of beam errors in high power laser diode bars and stacks," Opt. Express **14**(18), 8178–8183 (2006).
8. N. Trela, H. J. Baker, J. J. Wendland, and D. R. Hall, "Dual-axis beam correction for an array of single-mode diode laser emitters using a laser-written custom phase-plate," Opt. Express **17**(26), 23576–23581 (2009).
9. K. L. Wlodarczyk, I. J. Thomson, H. J. Baker, and D. R. Hall, "Generation of microstripe cylindrical and toroidal mirrors by localized laser evaporation of fused silica," Appl. Opt. **51**(26), 6352–6360 (2012).
10. E. Mendez, K. M. Nowak, H. J. Baker, F. J. Villarreal, and D. R. Hall, "Localized CO_2 laser damage repair of fused silica optics," Appl. Opt. **45**(21), 5358–5367 (2006).
11. P. Cormont, P. Combis, L. Gallais, C. Hecquet, L. Lamaignère, and J. L. Rullier, "Removal of scratches on fused silica optics by using a CO_2 laser," Opt. Express **21**(23), 28272–28289 (2013).
12. R. M. Brusasco, B. M. Penetrante, J. A. Butler, S. M. Maricle, and J. E. Peterson, "CO_2-laser polishing for reduction of 351-nm surface damage initiation in fused silica," SPIE Proc. **4679**, 34–39 (2001).
13. W. Dai, X. Xiang, Y. Jiang, H. J. Wang, X. B. Li, X. D. Yuan, W. G. Zheng, H. B. Lv, and X. T. Zu, "Surface evolution and laser damage resistance of CO_2 laser irradiated area of fused silica," Opt. Lasers Eng. **49**(2), 273–280 (2011).
14. T. D. Bennett, D. J. Krajnovich, L. Li, and D. Wan, "Mechanism of topography formation during CO_2 laser texturing of silicate glasses," J. Appl. Phys. **84**(5), 2897–2905 (1998).
15. T. D. Bennett, D. J. Krajnovich, and L. Li, "Thermophysical modeling of bump formation during CO_2 laser texturing of silicate glasses," J. Appl. Phys. **85**(1), 153–159 (1999).
16. T. D. Bennett and L. Li, "Modeling laser texturing of silicate glass," J. Appl. Phys. **89**(2), 942–950 (2001).
17. T. R. Shiu, C. P. Grigoropoulos, D. G. Cahill, and R. Greif, "Mechanism of bump formation on glass substrates during laser texturing," Appl. Phys. A **86**(3), 1311–1316 (1999).
18. "Corning® HPFS 7979, 7980, 8655 Fused Silica," *https://www.corning.com/emea/en.html*.
19. "Borofloat®33 – Borosilicate glass," *http://www.schott.com/borofloat/english/*.

#253539 Received 6 Nov 2015; revised 11 Jan 2016; accepted 12 Jan 2016; published 19 Jan 2016

20. P. Merz, H. J. Quenzer, H. Bernt, B. Wanger, and M. Zoberbier, "A novel micromachining technology for structuring borosilicate glass substrates," in *12th International Conference on Transducers, Solid-State Sensors, Actuators and Microsystems* (IEEE, 2003), pp. 258–261.
21. K. L. Wlodarczyk, *Surface deformation mechanisms in laser smoothing and micro-machining of optical glasses* (Ph.D. dissertation, Heriot-Watt University, 2011).
22. W. B. Pietenpol, "Surface tension of molten glass," J. Appl. Phys. **7**, 26–37 (1936).
23. W. D. Kingery, "Surface tension of some liquid oxides and their temperature coefficients," J. Am. Ceram. Soc. **42**(1), 6–10 (1959).
24. H. L. Schick, "A thermodynamic analysis of the high temperature vaporization properties of silica," Chem. Rev. **60**(4), 331–362 (1960).
25. E. Mendez Fernandez de Cordoba, *Laser micro-polishing of silica optics* (Ph.D. dissertation, Heriot-Watt University, 2007).
26. M. D. Feit, M. J. Matthews, T. F. Soules, J. S. Stolken, R. M. Vignes, S. T. Yang, and J. D. Cooke, "Densification and residual stress induced by CO_2 laser-based mitigation of SiO_2 surfaces," Proc. SPIE **7842**, 78420O (2010).
27. A. Q. Tool, "Relation between inelastic deformability of thermal expansion of glass in its annealing range," J. Am. Ceram. Soc. **29**(9), 240–253 (1946).
28. F. Wyrowski and O. Bryngdahl, "Iterative Fourier-transform algorithm applied to computer holography," J. Opt. Soc. Am. A **5**(7), 1058–1065 (1988).
29. P. J. Stepien, "Computer-generated holograms and diffraction gratings in optical security applications," Proc. SPIE **3973**, 224–230 (2000).
30. H. J. Baker, P. A. Field, F. Villarreal, S. D. Stratton, R. J. Ramirez, and D. R. Hall, "Line stabilization of slab waveguide CO_2 lasers and the laser signature revisited," Proc. SPIE **5120**, 55–59 (2003).
31. H. J. Baker, G. A. J. Markillie, P. Field, Q. Cao, C. Janke, and D. R. Hall, "Precision laser processing of optical microstructures with slab waveguide CO_2 lasers," Proc. SPIE **3888**, 625–634 (2000).
32. T. R. Steyer, K. L. Day, and D. R. Huffman, "Infrared absorption by small amorphous quartz spheres," Appl. Opt. **13**(7), 1586–1590 (1974).
33. "Operating manual. Germanium acousto-optic modulator. Model number: 37027-5," *http://www.goochandhousego.com/wp-content/uploads/2014/01/51A140021.pdf*.
34. H. Kogelnik and T. Li, "Laser beams and resonators," Appl. Opt. **5**(10), 1550–1567 (1966).

1. Introduction

Recently, we have developed a laser-based process for the direct writing of unique identification markings (holographic structures) on the surface of high value metals, such as stainless steel, nickel and nickel-chromium (Inconel®) alloys [1]. In contrast to the common approaches used for anti-counterfeiting marking of the metal products and components, i.e., polymer holographic stickers, which are attached to metals as an adhesive tape, the laser-generated identification markings are directly embedded to the metal surface and thus are robust to tampering and local damage. To generate the markings (holographic structures), we used 35ns laser pulses of wavelength 343nm to provide optically-smooth deformations on the metal surface using either a melt-only process or a combination of melting and vaporization, depending on the required depth of the hologram pixels.

The work described in this paper is focused on the development of a low-cost process for the generation of phase-only holographic structures on the surface of glass – a totally different material to that used in our previous work [1]. In contrast to other techniques commonly used for marking the glass substrates, such as mechanical engraving, sand blasting, laser engraving or etching [2, 3], our laser-based approach enables the flexible generation of robust and 'smart' markings without damaging the glass by fracturing (roughening) its surface. Instead of the generation of conventional markings, such as alphanumeric characters (serial numbers), bar codes, logos and 2D codes, our process enables the manufacture of 'hard-to-replicate' optically-smooth phase holographic structures that are capable of producing diffraction patterns containing text and/or images. In this work, we propose to use our process as an implementer of such unique security and anti-counterfeiting markings for the identification and traceability of high-value glass components and products. As explained in [1], phase holographic structures are more difficult to replicate than amplitude holographic structures, because the diffraction efficiency of the images generated by the phase holograms strongly depends on the shape and depth of the hologram pixels as well as the wavelength of light source (λ) used for revealing the diffractive image. In the case of binary phase holograms fabricated on transparent substrates, the maximum diffraction efficiency (i.e. diffractive image

#253539 Received 6 Nov 2015; revised 11 Jan 2016; accepted 12 Jan 2016; published 19 Jan 2016

without the 0th order beam) is obtained when the pixels are λ/2 deep and their shape is similar to square-shaped cavities with a flat bottom [1].

The process uses an inexpensive CO_2 planar waveguide laser that provides microsecond laser pulses of wavelength 10.59μm. This wavelength is particularly well-suited to the machining and polishing of glass as demonstrated in the manufacture both conventional and custom-made refractive optics [4–6] as well as for the fabrication of micro-optical components, e.g., phase corrective plates for high power laser diodes [6–8] and *micro-stripe* cylindrical and toroidal mirrors [9]. As demonstrated by Mendez *et al.* [10] and more recently by Cormont *et al.* [11], a CO_2 laser beam can also be used for repairing of damage in fused silica components by re-melting, or it can be used for enhancing the surface damage resistance of fused silica optics [12, 13]. Bennett *et al.* [14–16] and Shiu *et al.* [17] also demonstrated the use of a CO_2 laser beam for the generation of bumpy textures on the surface of various silicate glasses and explained the mechanism of their formation.

The holographic structures presented in this paper are generated on the surface of fused silica (HPFS®7980 Corning) and borosilicate (Borofloat®33 Schott AG) glass using a CO_2 laser spot of a diameter 35μm, pulses of duration 10μs, and peak powers of less than 20W to provide a combination of melting and evaporation. The holograms are written as an array of pixels arranged in an appropriate pattern, in which each of the pixels is an optically-smooth crater with a diameter of approximately 20μm and a peak-to-valley value of less than 500nm.

Fused silica is a well-known glass that is often used as a substrate for the manufacture of high precision optics for high average power lasers and optical devices, e.g. flat field F-theta lenses for galvo-scanning systems. HPFS®7980 Corning is a high purity synthetic fused silica glass that is characterized by a very low coefficient of thermal expansion (CTE = 0.55ppm/K), low refractive index variations ($\Delta n < 0.1$ for the λ range between 200nm and 1100nm), low birefringence, high hardness, and exceptional transmission from the deep ultraviolet (DUV) to the near-infrared (NIR) region [18]. Borofloat®33 was chosen as a test substrate because this borosilicate float glass is often used in many industrial and scientific areas, such as micro-electronics, chemistry, biotechnology, optics, lighting and photovoltaics [19, 20]. Borofloat®33 glass is characterized by similar optical properties to fused silica, but is less expensive. This colorless and optically flat glass is highly transparent in the visible and NIR spectral range (from 400nm to 2.5μm). It is also highly resistant to thermal shock (CTE = 3.3ppm/K) and to chemicals such as strong acids, alkalis and organic substances.

2. Experimental setup

The customized CO_2 laser micromachining system used in the work described in this paper is shown schematically in Fig. 1. The system is based on a commercial 300W average power CO_2 planar waveguide laser (Rofin-Sinar SCx20, UK) that can provide millisecond and microsecond RF excitation pulses of a nominal wavelength 10.59μm. In our work, the laser was set up to generate pulses of duration τ_L = 200μs at a pulse repetition frequency (PRF) of 200Hz. At these settings, the average output laser power (P_{OUT}) was measured to be 30W, providing a peak power (P_{Pk}) of 750W. The P_{PK} value was reduced to approximately 35W using ZnSe beam splitters.

The laser beam delivered to the workpiece was provided from the first diffraction order beam generated by a germanium-crystal acousto-optic modulator (NEOS Technologies, US). The modulator enabled accurate control of the peak power delivered to the workpiece, by adjusting the AOM voltage, as well as shortening on-demand the duration of laser pulses (in the range between 1μs and 200μs). Shorter laser pulses were obtained by providing a gating signal to the AOM, as illustrated in Fig. 2(a). The peak power (P_{Pk}) as a function of the AOM voltage for various durations of the AOM gating signal (τ_{AOM}) and a constant delay (τ_D = 50μs) between the laser triggering signal and the AOM signal is shown in Fig. 2(b).

#253539 Received 6 Nov 2015; revised 11 Jan 2016; accepted 12 Jan 2016; published 19 Jan 2016

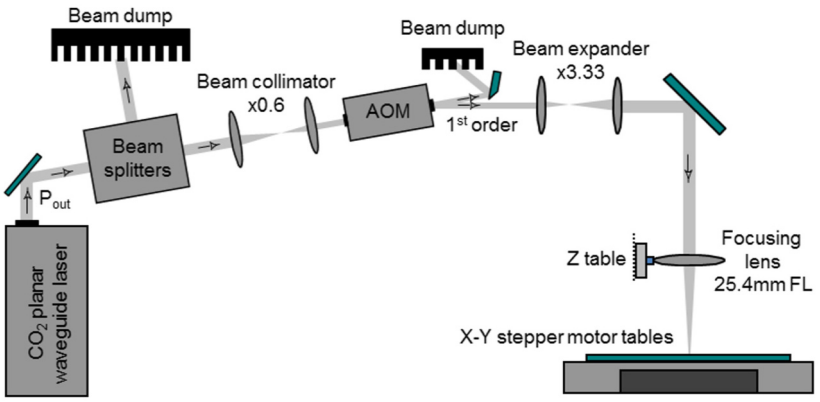

Fig. 1. Customized CO_2 laser micromachining system.

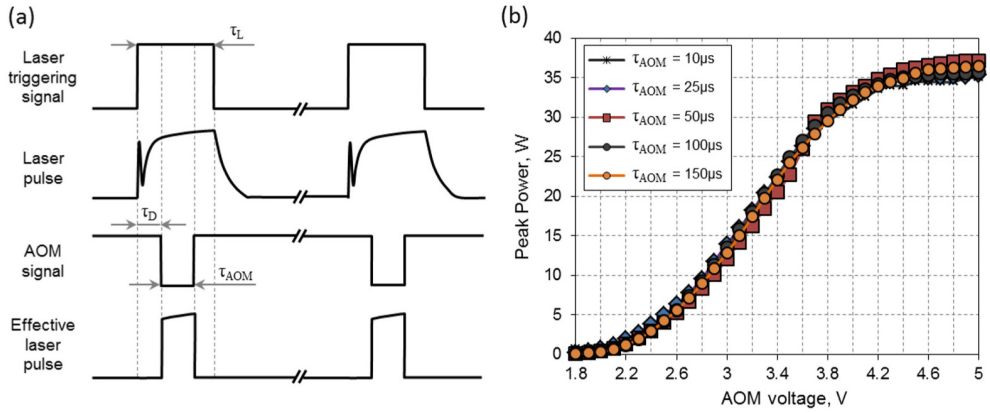

Fig. 2. (a) Control of the duration of laser pulses using AOM, (b) Peak power on the workpiece as a function of the AOM voltage for various duration of the AOM gating signal (τ_{AOM}) and a constant delay τ_D = 50μs.

The aperture of the AOM was 5mm, so the output laser beam diameter ($2\omega_0 = 8 \pm 0.5$mm, $M^2 < 1.2$) had to be reduced by a factor of 0.6, achieved by using a telescope formed of two ZnSe meniscus lenses with focal lengths (FLs) of 63.5mm and 38.1mm. The optical losses of the AOM (germanium) crystal were measured to be 11%, whereas the maximum diffraction efficiency of the AOM was 81%. The optical losses of the crystal were defined as: $L = \Delta P/P_{INC}$, where ΔP was a difference between the optical power of the incident laser beam (P_{INC}) and the sum of the zero order (P_0) and the first order diffracted (P_1) beams. The diffraction efficiency was defined as follows: $\eta = P_1/(P_0 + P_1)$.

One of the aims in this project was to manufacture holographic structures with a relatively small pixel diameter in order to produce holograms that are as small as possible and also importantly to maximize their diffractive angle. We managed to achieve an approximately 35μm diameter laser spot on the workpiece by transmitting the deflected (first order) laser beam through a × 3.33 beam expander, that contained two ZnSe lenses with FLs of 38.1mm and 127mm, and a focusing (ZnSe aspheric) lens with a FL of 25.4mm. Since the deflected laser beam was elliptical, the circular spot on the workpiece was obtained by slightly defocusing the beam. The focusing lens was mounted on a stepper motor stage providing 100mm travel range with a step resolution of 0.5μm and a repeatability of 1μm.

The transverse (X-Y) movement of the workpiece during laser micromachining was provided by two further stepper motor stages. One of these was identical to that used for moving the focusing lens, whilst the other, with a travel range of 50mm, provided movement

#253539 Received 6 Nov 2015; revised 11 Jan 2016; accepted 12 Jan 2016; published 19 Jan 2016

with a step resolution of 0.1μm and a repeatability of 1μm. In general, the X-Y stepper motor tables ensured accurate movement of the workpiece with a sub-micrometer resolution, whereas the AOM enabled on-demand firing of laser pulses of specific duration and peak power. This approach allowed arbitrary texture designs to be precisely mapped 'point-by-point' onto the workpiece surface.

3. Characterization of CO_2 laser-induced surface deformations on glass substrates

Two of the most commonly-used optical glass substrates, high purity fused silica (HPFS®7980 Corning) and borosilicate (Borofloat®33 Schott) glass, were tested. The fused silica samples were 1mm thick, whereas the borosilicate samples had a thickness of 1.1mm. Prior to the laser treatment, the samples were carefully cleaned using methanol and lens tissues in order to remove any dust and contamination.

A detailed analysis of the CO_2 laser-induced deformations on the surface of the glass substrates was performed using a white-light source interferometer (Zygo). This instrument enabled measurement of the deformations with a lateral (spatial) resolution of about 100nm and a vertical resolution of <1nm.

3.1 Results

Laser peak powers (P_{PK}) up to several hundred Watts and pulse durations in the range of 1-150μs were used in our experiments. In general, it was found that shorter laser pulses generate a smaller heat-affected zone (HAZ) within the laser-irradiated area and thus the glass substrate is less prone to cracking – a particular issue with borosilicate glass that has a coefficient of thermal expansion (CTE) 5 times higher than fused silica. To avoid cracking in borosilicate glass it is best to use a pulse length ≤ 10μs and a peak power P_{PK} < 35W. These laser processing parameters were determined experimentally by analyzing a large number of calibration maps performed for both glass samples using laser pulses of various durations (in the range of 1-150μs) and peak powers (up to several hundred Watts). The calibration maps (similar presented in [10, 21]) were analyzed in terms of the shape, depth, diameter of the laser-induced surface deformations as well as the presence of cracking, using the Zygo profilometer and an optical microscope (Leica), respectively.

In order to create optically smooth dimples it is also important to avoid significant 'melt eject' which can result in the creation of 'splashes' of melt re-welded to the surface around the dimple. This tends to occur at higher peak power levels e.g. on borosilicate glass such features are generated with P_{PK} > 25W for a 35μm laser spot, with 10μs pulses.

Figure 3 shows examples of laser-created dimples produced on the surface of the fused silica glass substrate. Each was produced using a single laser pulse of duration 10μs. Figure 3(a) shows a deformation produced just above threshold, for P_{PK} ≈17W, whilst Figs. 3(b) and 3(c) show examples created with higher peak powers. The threshold here is defined as the onset of appearance of the laser-induced surface deformations detectable by the Zygo profilometer.

#253539 Received 6 Nov 2015; revised 11 Jan 2016; accepted 12 Jan 2016; published 19 Jan 2016

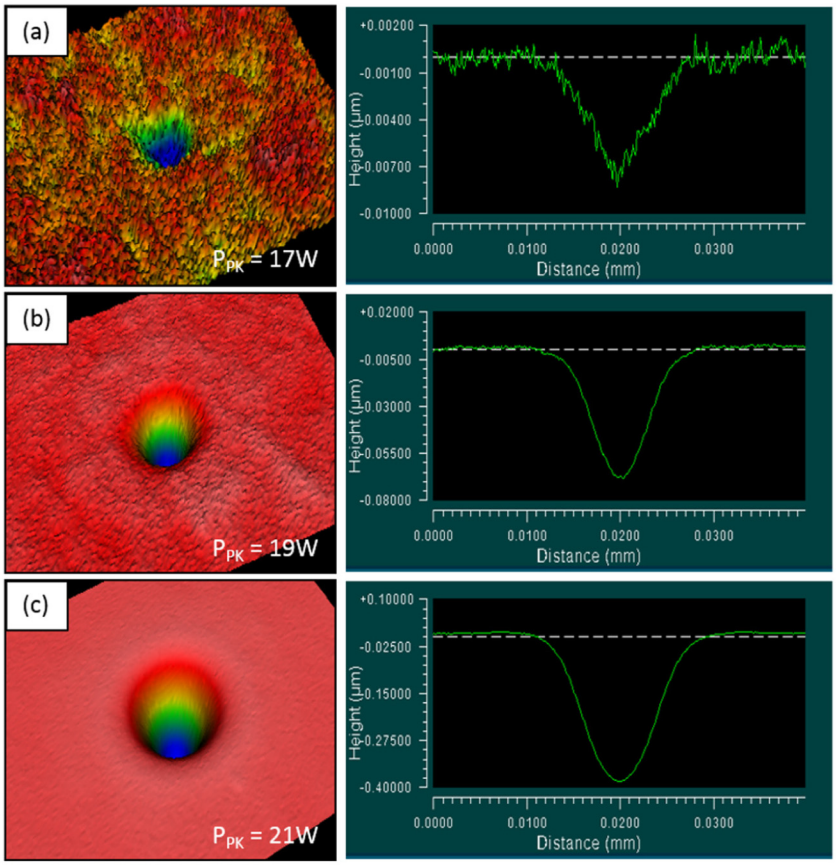

Fig. 3. CO_2 laser-induced deformations on the surface of HPFS®7980 Corning glass substrate near the threshold. Pulse duration was 10µs, whereas the peak power was: (a) 17W, (b) 19W, and (c) 21W.

The laser-induced surface deformations on borosilicate were quite different to those on fused silica, as shown in Fig. 4. The laser peak power threshold (P_{PK} ≈4.5W) was only a quarter that for fused silica. In the range of peak powers between 4.5 and 7W, the deformations were observed to be protrusions ('*dome-shaped*' bumps), as can be seen in Fig. 4(a), rather than craters. As the peak power was further increased to 7.5W, these bumps were observed to have a little dimple in the center, as shown in Fig. 4(b). This dimple was transformed into a crater for further increases in peak power, as shown in Figs. 4(c) and 4(d). As with the fused silica sample, the laser-generated craters on the borosilicate glass surface were optically smooth. However, their shape was different in that they were surrounded by an elevated rim, as can be seen in Fig. 4(d). The height of this rim never exceeded 200nm.

#253539 Received 6 Nov 2015; revised 11 Jan 2016; accepted 12 Jan 2016; published 19 Jan 2016

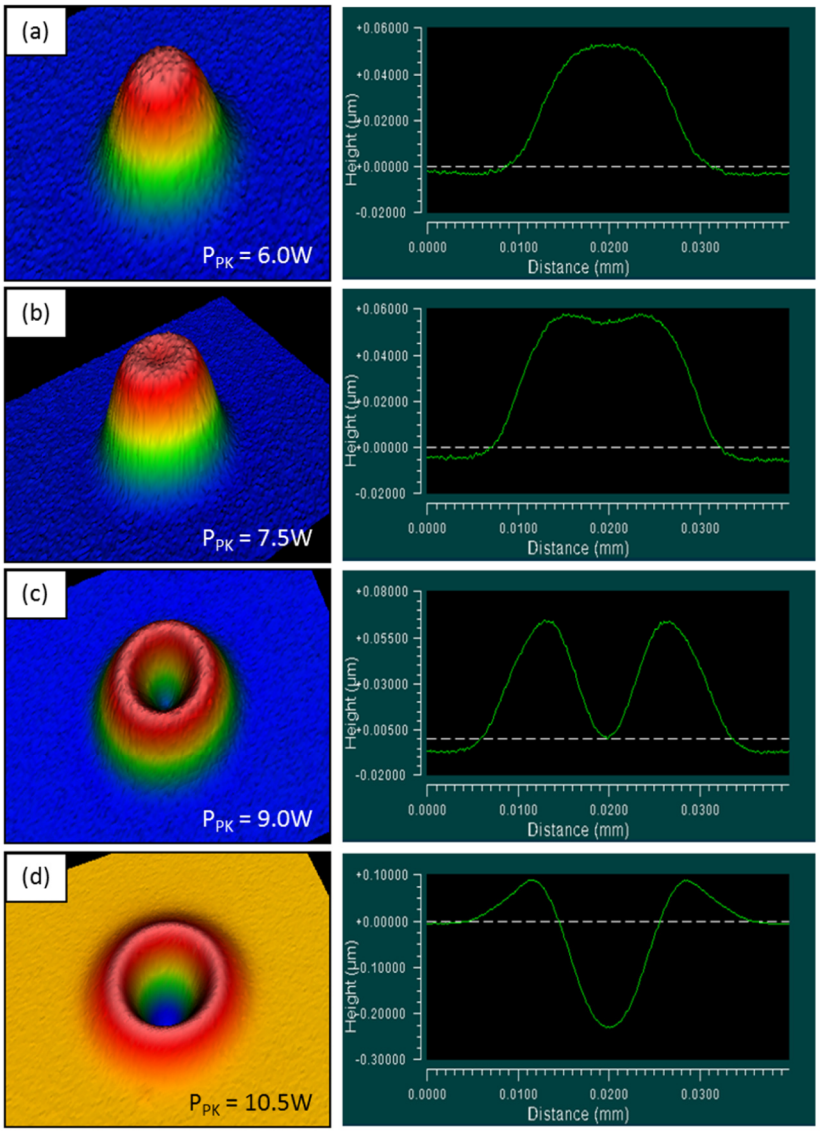

Fig. 4. CO_2 laser-induced deformations on the surface of borosilicate glass substrate near the threshold. Pulse duration was 10µs, whereas the peak power was: (a) 6.0W, (b) 7.5W, (c) 9.0W and (d) 10.5W.

In Fig. 5 the depth and diameter of the laser-induced deformations produced on the surface of the fused silica and borosilicate glasses are plotted as a function of laser peak power. These deformations were generated using single laser pulses of duration 10µs and a laser spot of diameter 35µm. The depth of the deformations was measured as a height difference between the untreated surface level and the center of the deformations. The '*dome-shaped*' and '*doughnut-shaped*' bumps seen close to the threshold with borosilicate, as shown in Figs. 4(a)–4(c), are defined as having a negative depth. In general, Fig. 5(a) shows that the depth of the craters increases linearly with increasing peak power, both in fused silica and borosilicate glass. The horizontal error bars are the consequence of the laser power fluctuations (discussed later in Section 5), whereas the vertical error bars are the standard deviations of the depth measurement calculated for two sets of craters produced with the same values of the AOM voltage.

#253539 Received 6 Nov 2015; revised 11 Jan 2016; accepted 12 Jan 2016; published 19 Jan 2016

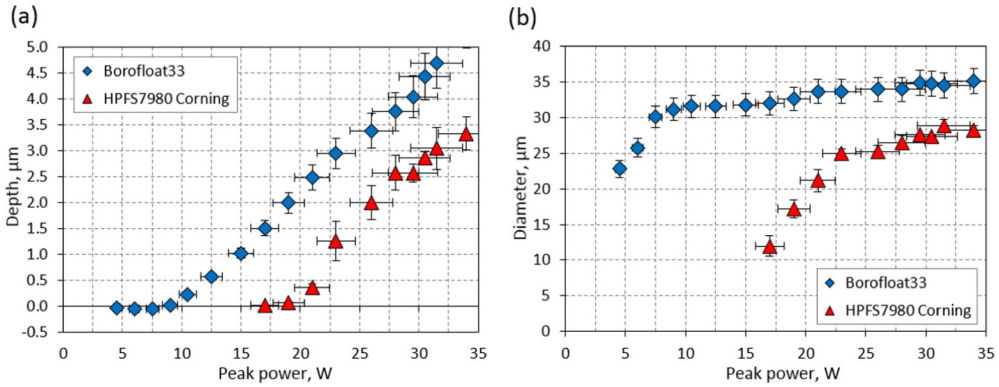

Fig. 5. (a) Depth and (b) diameter of the CO_2 laser-induced deformations (craters and bumps) produced on the surface of fused silica (HPFS®7980 Corning) and borosilicate (Borofloat®33) glasses as a function of the peak power. The deformations were generated using single laser pulses of duration 10µs and a laser spot of diameter 35µm.

3.2 Glass annealing and results discussion

Three possible processes are expected to be involved in the generation of the laser-induced surface deformations presented in Section 3.1, i.e. (i) melting; (ii) vaporization; and (iii) density changes caused by a localized increase of fictive temperature (see below). In order to distinguish the deformations produced by pure melting from those in which vaporization was also involved, and importantly to determine the onset of glass vaporization, it was necessary to first of all remove the density changes, by annealing the glass samples in a furnace (Nabertherm model LF15/13). This allowed the change in material volume due to vaporization to be calculated. The fused silica sample was heated to 1042°C (the annealing point) at a rate of 10°C/min, held at this temperature for 1 hour, and then slowly cooled down to 850°C (below the strain point) at a rate of 2°C/min, and subsequently down to room temperature at a rate of 10°C/min. The borosilicate glass was annealed following a similar temperature profile; this time, however, the annealing point was 560°C, and the temperature at which the cooling rate was increased was 470°C. After the annealing process, the laser-induced surface deformations were re-measured using the Zygo surface profilometer, with the results shown in Figs. 6 and 7 for fused silica and borosilicate, respectively.

#253539 Received 6 Nov 2015; revised 11 Jan 2016; accepted 12 Jan 2016; published 19 Jan 2016

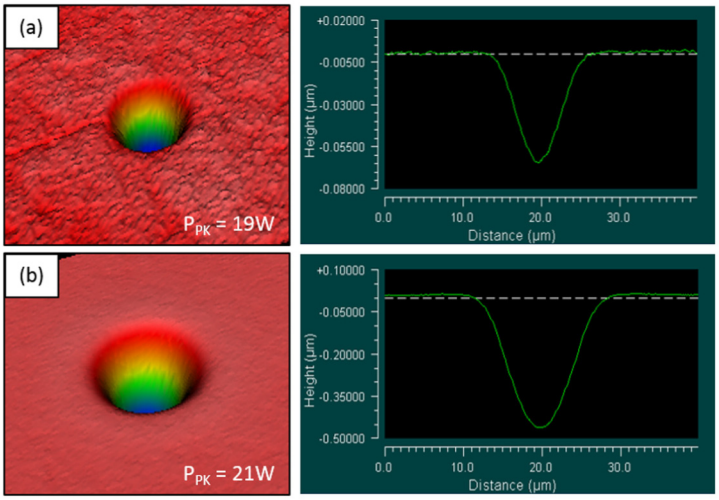

Fig. 6. CO_2 laser-induced deformations on the surface of fused silica glass after annealing at 1042°C for 1 hour. Deformations before annealing are shown in Fig. 3.

#253539 Received 6 Nov 2015; revised 11 Jan 2016; accepted 12 Jan 2016; published 19 Jan 2016

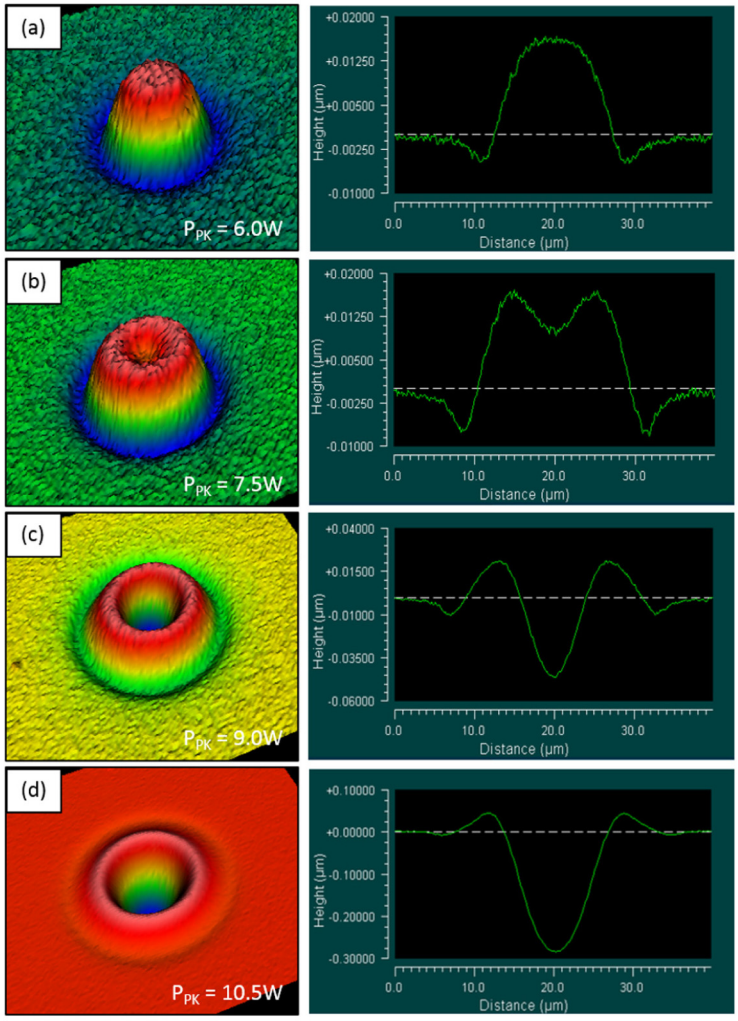

Fig. 7. CO_2 laser-induced deformations on the surface of borosilicate glass after annealing at 560°C for 1 hour. Deformations before annealing are shown in Fig. 4.

The 7nm deep dimple generated on the surface of fused silica at P_{PK} = 17W, as can be seen in Fig. 3(a), could no longer be detected by the Zygo surface profilometer after the annealing process, i.e., a flat surface was measured. The other craters generated on the fused silica surface at higher peak powers (P_{PK} > 17W) after annealing were almost identical in shape to those before annealing. With borosilicate, however, the laser-induced surface deformations looked significantly different after annealing, as can be seen by comparing Figs. 4 and 7. By calculating the overall change in volume for a range of peak powers, as plotted in Fig. 8, the onset of vaporization can be estimated to be P_{PK} = 9W. With fused silica, meanwhile, the reduced melt flow effects mean that the vaporization threshold can be estimated directly from Figs. 3 and 6, to be P_{PK} between 17W and 19W.

#253539 Received 6 Nov 2015; revised 11 Jan 2016; accepted 12 Jan 2016; published 19 Jan 2016

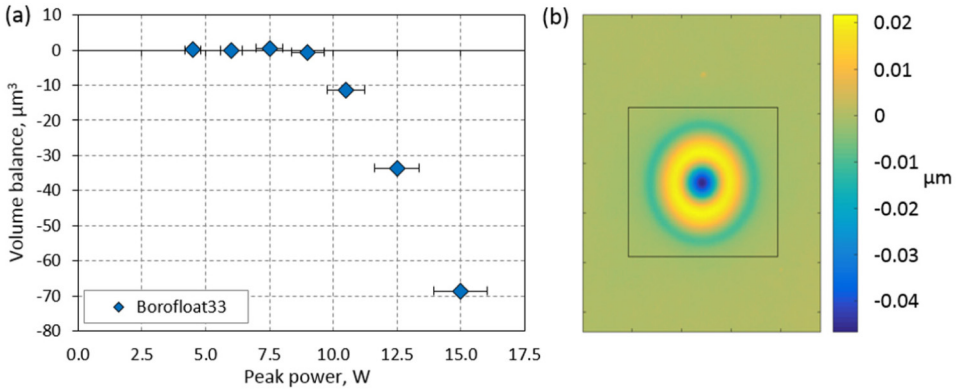

Fig. 8. (a) Overall volume change calculated for the annealed borosilicate glass. (b) Surface profile of the deformation produced with P_{PK} = 9.0W including the highlighted area (square) selected for the calculation of the volume change.

The shape changes observed in borosilicate on annealing demonstrate that even below the vaporization threshold, two mechanisms are involved in the generation of surface structures: the *Marangoni* effect and the *fictive temperature* effect, with the second of these explaining the changes that occur on annealing. The *Marangoni* effect determines the direction of flow of the molten glass layer that is driven by the gradient of surface tension [22]. Depending on whether the surface tension gradient is positive or negative, this leads to the formation of either a protrusion or a depression within the molten area. In the case of the borosilicate glass sample, the gradient of surface tension was positive and therefore the molten layer of glass was pulled towards the centre of the laser-irradiated area (the hottest site). The positive gradient of surface tension in borosilicate glass results from the tendency of the main constituents of this glass, i.e., SiO_2 and B_2O_3, to dissociate at elevated temperatures [23, 24]. In the case of the fused silica sample, meanwhile, the *Marangoni* effect was unnoticeable. Based on the results presented by E. Mendez [25], the surface deformations induced by the *Marangoni* effect only become significant in fused silica when the interaction time between the glass and the laser beam is greater than tens of microseconds, i.e. when a wider and deeper melt pool is generated.

The *fictive temperature* effect alters the density and hence the volume of glass within the laser-irradiated area, as reported by many researchers [14–17, 26]. The fictive temperature is a term proposed by Tool [27], who suggested that glass that is cooled through the transformation range, i.e. the range in which glass becomes a solid, has an identical frozen-in structure to that of its melt at some equilibrium temperature. Depending on the cooling rate of glass in the transformation range, the glass network undergoes either faster or slower structural changes, and thus the value of fictive temperature is modified. In general, glass that is cooled slowly has a lower fictive temperature than the same glass that is cooled rapidly.

Commercial glasses have a low fictive temperature, somewhere between the strain point and the annealing point, because they are cooled slowly in the manufacturing process in order to minimize the thermally-induced stresses. However, the value of fictive temperature can be increased, even up to the softening point, if glass is re-heated above the annealing point and then rapidly cooled down through the transformation range. With the laser process considered here the cooling rate can be very high (more than 10^4K/s), resulting in a high fictive temperature within the laser-irradiated area. This means that some physical properties of the glass samples (e.g. refractive index and density) are typically modified in this region. The effect of an increase of the fictive temperature in many silicate glasses was demonstrated by Bennett *et al.* [14–16] and Shiu *et al.* [17]. They showed that the laser-induced increase of fictive temperature *decreases* the density of these glasses within the laser-irradiated area. This leads to the *increase* of the glass volume in this region and the creation of deformations in the form of bumps on the glass surface.

#253539 Received 6 Nov 2015; revised 11 Jan 2016; accepted 12 Jan 2016; published 19 Jan 2016

The results presented in Figs. 7(a)–7(c) show clearly that the dimension of the protrusions is reduced when the borosilicate sample is annealed because the original (low) value of the fictive temperature was restored. With fused silica, however, an increase of fictive temperature was expected to have the opposite effect, resulting in densification and thus the generation of a shallow depression within the laser-irradiated area, as observed in our previous works [9, 21]. Such a densification was observed near the vaporization threshold at P_{PK} = 17W as seen in Fig. 3(a), where the 7nm deep dimple was removed after annealing. However, it is clear that the fused silica sample used in this work was less susceptible to the laser-induced densification than the fused silica substrate used in [9], most likely because of a much smaller laser spot (35µm compared to a 1mm diameter spot) and shorter interaction time (~10µs compared to the tens of milliseconds) between the glass and the laser pulses.

4. Generation of holographic structures

As shown in the previous section, optically smooth craters on the surface of fused silica and borosilicate glass can be generated by a combination of vaporization and melting. Moreover, it was demonstrated that the depth of these craters increases almost linearly with increasing peak power, as shown in Fig. 5(a), due to strong linear absorption of these glasses at the wavelength of 10.6µm, making CO_2 laser pulses suitable for the generation of various optical structures (e.g. holograms) on the glass surface.

4.1 Design and fabrication

The design and fabrication process of the holographic structures on the surface of glass is illustrated in Fig. 9. The design procedure of the holograms was identical to that described in our earlier work [1]. Information in the form of an image and/or alphanumeric characters that will be carried by a hologram can be designed using a simple graphical tool (MS Paint). Such a design (e.g. a black & white image containing an 'AOP' inscription – an acronym of the 'Applied Optics & Photonics' research group at Heriot-Watt University) is processed using the IFTA (Iterative Fourier Transform Algorithm) [28] in order to generate a two-level (binary) phase computer generated hologram (CGH) [29]. To increase an effective aperture of the holographic structure, the designed hologram is copied several times and tiled in an '$m \times n$' arrangement. Such a tiled hologram is finally mapped onto the surface of a glass substrate using a CO_2 laser beam.

The IFTA was optimized for designing (ideal) CGHs containing square-shaped pixels with a flat bottom. In the case of phase CGHs, it is very important to use a light source of an appropriate wavelength (λ) for illuminating the holographic structure in order to obtain the maximum diffraction efficiency (contrast) of the diffractive image generated by the hologram. For the ideal binary CGHs, the maximum diffraction efficiency (with a lack of the 0th order beam) is obtained when the depth of the hologram pixels generated on a glass substrate is equal to λ/2.

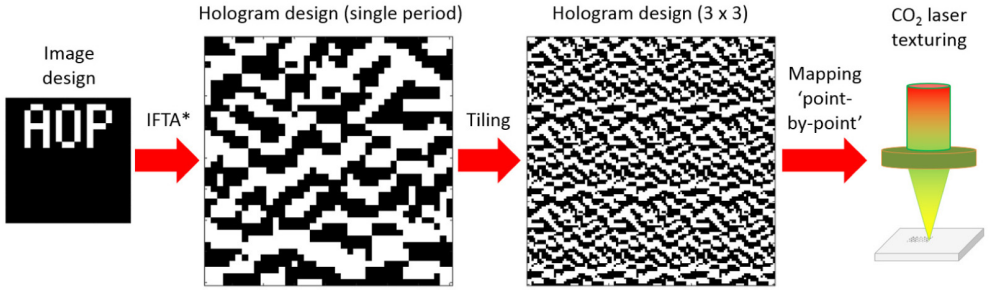

Fig. 9. Design and fabrication process of holographic structures on glass.

An example of the holographic structure that was generated on the surface of a 1.1mm thick borosilicate glass substrate is shown in Fig. 10. The hologram pixels were generated

#253539 Received 6 Nov 2015; revised 11 Jan 2016; accepted 12 Jan 2016; published 19 Jan 2016

using laser pulses of a duration 10μs and a peak power of 12.5W. The distance between the consecutive hologram pixels was chosen to be 24μm, so the laser-generated craters did not overlap each other and undesirable valleys between the pixels were avoided. The hologram pixels were evenly spaced in both (X and Y) directions, as can be seen in Fig. 10(b). A characteristic feature of the hologram pixels generated on the borosilicate glass surface is the elevated rim around the craters observed earlier (see Section 3). The height of these rims does not exceed 200nm.

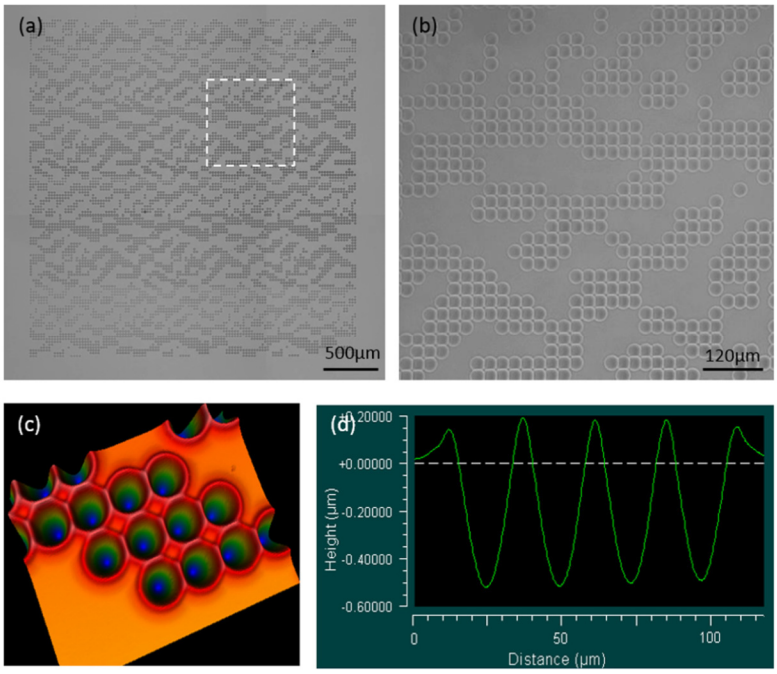

Fig. 10. Holographic structure produced on the surface of borosilicate glass: (a) optical microscope image, (b) close-up of the selected area, (c) 3D surface profile and (d) cross section of the hologram pixels, measured using the Zygo profilometer. Peak power was 12.5W.

Various holographic structures were also generated on the surface of fused silica and an example of such a structure, consisting of craters of depth 400nm, is shown in Fig. 11. The peak power used for the generation of this structure was 21W. The distance between the crater centers (hologram pixels) was 20μm in this case. The smaller spacing was possible because the craters in fused silica do not have an elevated rim.

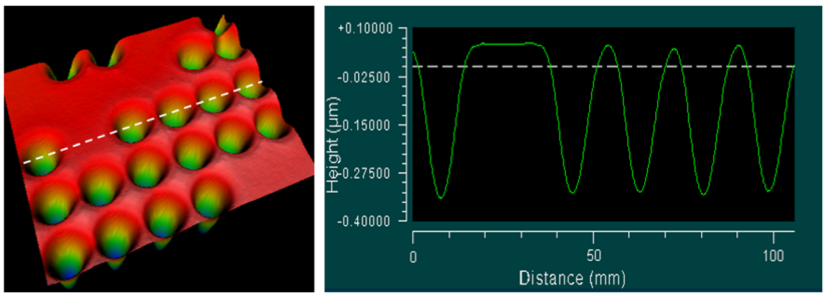

Fig. 11. 3D surface profile and cross section of the hologram pixels generated on the surface of fused silica, measured using the Zygo profilometer. Peak power was 21W.

#253539 Received 6 Nov 2015; revised 11 Jan 2016; accepted 12 Jan 2016; published 19 Jan 2016

4.2 Testing

The optical performance of the holographic structures generated on the glass substrates was tested using two techniques. In the first setup, which is shown in Fig. 12(a), we used a collimated laser beam of a wavelength 532nm (green) that was provided from a low-cost laser pointer. This was used to illuminate the hologram surface and the diffractive image generated by a hologram was projected onto a screen located a few meters away from the hologram surface, as shown in Fig. 12(a). An example of the diffractive image generated in this setup is presented in Fig. 12(b). This particular image was generated by the holographic structure shown in Fig. 10. As can be seen in Fig. 12(b), the diffractive image contains the expected 'AOP' inscription, but also the 0th order beam and a '*twin*' image (the second 'AOP' inscription) that is rotated with respect to the other by 180 degrees. The presence of the 0th order beam and the '*twin*' image results from the '*Gaussian-like*' shape of the hologram pixels, as concluded by performing the simulations described in [1].

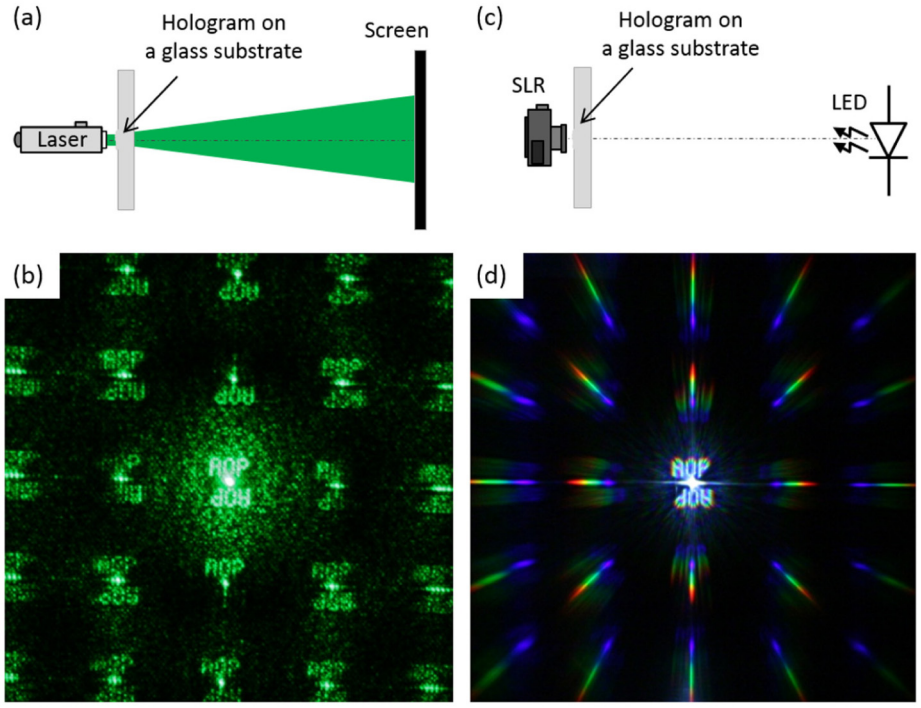

Fig. 12. Testing the CO_2 laser generated holographic structures: (a) using a laser beam and (c) an LED. Examples of the diffractive images generated by the holograms in the setups (a) and (c) are shown in (b) and (d), respectively.

The second setup that was used for testing the optical performance of the holographic structures is shown in Fig. 12(c). In this simple setup, we used a broadband light source (LED) that was available in a flashlight of a smartphone. To record the diffractive image generated by the hologram, the white light source (smartphone) was placed a few meters away from the hologram surface, whereas an SLR camera focused on the source was located just behind the hologram. Figure 12(d) shows the diffractive image generated by the holographic structure presented earlier in Fig. 10. This diffractive image contains the AOP inscription, the 0th order beam and the '*twin*' image. However, it is not affected by speckle interference, unlike that in Fig. 12(b), which results from the high coherence of the laser beam used in the previous setup.

#253539 Received 6 Nov 2015; revised 11 Jan 2016; accepted 12 Jan 2016; published 19 Jan 2016

5. Influence of laser wavelength instability on the performance of the holograms

The long-term power stability of the CO_2 laser used (Rofin SCx20, after a 2-hour warm-up time) is approximately ± 7%, in-line with the laser specification. As reported in our previous work [21], the laser power fluctuations are strongly correlated with the laser wavelength instability. In general, the laser had a tendency to change spectral lines quite frequently (multiple times within an hour) and even to operate on multiple wavelengths (in the range between 10.25µm and 10.63µm). As reported elsewhere [30], planar waveguide CO_2 lasers with an unstable resonator can operate at multiple wavelengths and the line-hopping effect is very often observed in such lasers.

There are several sources that can cause the change of a nominal laser wavelength (line-hopping) and hence the laser power fluctuations. For instance, the line-hopping effect may result from the thermal fluctuations within the laser cavity, affecting on the physical length of the resonator [31]. As reported in [30], line hops or mode hops may also occur within an individual RF-discharged pulse as the gas in the laser resonator expands.

During this project, it was found that the wavelength stability of the CO_2 laser is very important because it has a significant impact on the performance of the holographic structures generated on a glass substrate. The optical properties of many glass substrates are dependent on the wavelength. For instance, the reflectivity of fused quartz (Vitrosil®) at $\lambda = 10.23\mu m$ is approximately 60% greater than that at $\lambda = 10.59\mu m$ [21, 32]. This means that the laser energy coupled into the glass varies for different wavelengths. In our work, it was also found that the change of the laser wavelength may introduce a significant beam positioning error on the workpiece, causing generation of the unevenly-spaced hologram pixels on the glass surface. This is because laser beams of different wavelengths are deflected with different angles by the the AOM. The deflection angle (Φ_d) can be calculated using the following equation [33]: $\Phi_d = (f_A\lambda) / (2V)$, where f_A is an acoustic drive frequency (27.12MHz), λ is the laser wavelength, and V is an acoustic velocity of the germanium crystal (5500m/s). This means that the laser beam on the glass workpiece can be shifted by up to 6.5µm when the laser wavelength is changed to the extreme wavelength of 10.25µm. This beam positioning error was estimated using the ABCD matrix method [34].

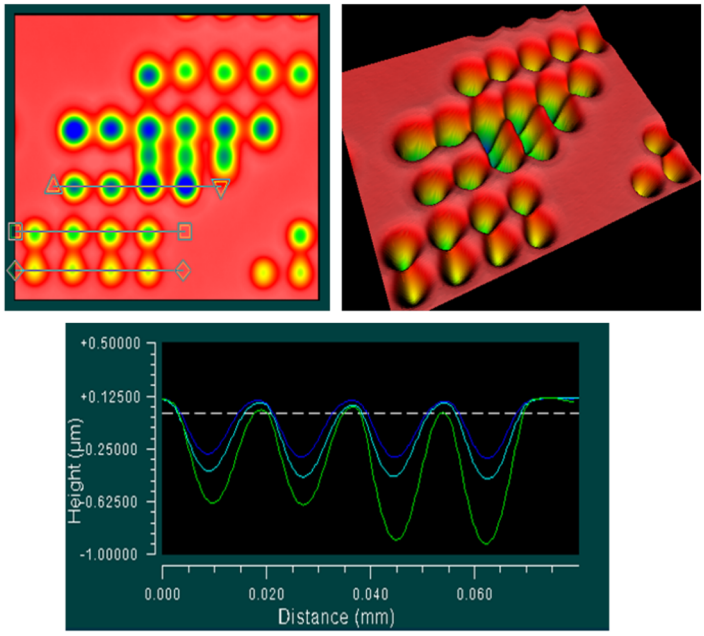

Fig. 13. Imperfections in the holographic structure resulting from the laser wavelength hopping.

#253539 Received 6 Nov 2015; revised 11 Jan 2016; accepted 12 Jan 2016; published 19 Jan 2016

Figure 13 shows the consequences of laser wavelength hopping which occurred during the generation of a holographic structure on the surface of the fused silica sample. Here, it can be seen that the depth of the hologram pixels varies in each row and the hologram pixels are not evenly spaced. Also, some hologram pixels are not circular, which means that they were produced when the laser was operating at multiple wavelengths.

6. Conclusions and future work

In this paper, we describe and evaluate a novel laser-based approach for the generation of holographic structures, formed of arrays of optically-smooth craters, on the surface of fused silica and borosilicate (Borofloat®33) glass substrates. A customized CO_2 laser-based micromachining system was used to enable the generation of 'square-shaped' laser pulses of a precisely defined duration and peak power. The generated holograms could form the basis of hard-to-replicate anti-counterfeiting marks, and their optical performance was presented in this paper. The results presented in Section 5 suggest that our future work should be focused on the development of an efficient method for the stabilization of laser wavelength in order to avoid the line hopping effect during the writing process of holograms.

Acknowledgments

The research covered in this paper was funded by the Engineering and Physical Sciences Research Council (EPSRC): Centre for Innovative Manufacturing in Lased-based Production Processes (Grant No: EP/K030884/1), and Renishaw plc. (UK).

#253539 Received 6 Nov 2015; revised 11 Jan 2016; accepted 12 Jan 2016; published 19 Jan 2016